Journal of the Optical Society of America B
OPTICAL PHYSICS

Flexible random lasers in dye-doped bio-degradable cellulose nanocrystalline needles

Gleice C. M. Germano,[1,†] Yan D. R. Machado,[1,†] Lucas Martinho,[1] Susete N. Fernandes,[2] Antonio Mario L. M. Costa,[3] Edison Pecoraro,[4] Anderson S. L. Gomes,[5] and Isabel C. S. Carvalho[1,*]

[1]Physics Department, Pontifical Catholic University of Rio de Janeiro, Rio de Janeiro 22451-900, Brazil
[2]i3N/CENIMAT, Department of Materials Science, Faculty of Science and Technology, Universidade NOVA de Lisboa, Campus de Caparica, 2829-516 Caparica, Portugal
[3]Department of Chemical and Materials Engineering, Pontifical Catholic University of Rio de Janeiro, Rio de Janeiro 22451-900, Brazil
[4]Institute of Chemistry, UNESP-São Paulo State University, Araraquara, SP 14800-060, Brazil
[5]Physics Department, Universidade Federal de Pernambuco, Recife-PE 50670-901, Brazil
*Corresponding author: isabel.carvalho@puc-rio.br

Received 14 August 2019; revised 9 November 2019; accepted 11 November 2019; posted 11 November 2019 (Doc. ID 375396); published 4 December 2019

In this work, we developed and investigated a random laser based on rhodamine6G (Rh6G) in ethylene glycol (EG) solution with varying cellulose nanocrystalline (CNC) needles as scatterers in the lasing media. Besides the suspension-in-cuvette scheme, an alternative configuration was also employed: a dye-CNC flexible self-supported thick-film (70 μm) random laser made by drop casting of the CNCs + Rh6G + hydroxypropyl cellulose suspension. In relation to conventional scatterers, the biodegradable cellulose nanocompounds showed a comparable reduction in both the spectral full width at half-maximum and the energy threshold values, with an optimal concentration of 5 mg [CNC]/ml[EG] in suspension. Its performance was also compared with other cellulose-based random lasers, presenting advantages for some parameters. The flexible film configuration showed similar results, but contained 10% less Rh6G than the suspension.

https://doi.org/10.1364/JOSAB.37.000024

1. INTRODUCTION

Cellulose-based nanostructures have attracted a great deal of attention due to their increasing number of photonic applications in devices related to light generation, guiding, detection, amplification, and confinement [1–4]. Coherent emission cellulose-based optical sources have been demonstrated in the form of random lasers (RLs). The RL is a low-coherence photon source in which the optical feedback relies on scattering processes in nano- or submicrometer structured media, instead of a conventional mirror-based Fabry–Perot cavity. The RL has attracted a great deal of attention in the last decades, as reviewed in [5–7], after its first clear experimental demonstration in 1994 [8], over two decades after Lethokhov's theoretical proposal of such a coherent light source [9]. Different gain media may be appropriately pumped to provide the required ingredients for laser emission, which include dyes, semiconductors, polymers, quantum dots, and rare-earth ions [5]. The scattering media in the RLs are generally submicrometer or nanosized materials, either dielectric (TiO_2, Al_2O_3), semiconductors (ZnO), rare-earth doped glasses and nanocrystals (Nd, Er), or metallic nanomaterials (e.g., Au, Ag), in which case, localized surface plasmons play an important role [5]. It is important to mention that random fiber lasers, whereby optical fibers are employed as the guiding media, have been demonstrated since 2007 [10], as reviewed in Ref. [11]. It is important to differ random fiber lasers [10,11], which employ the gain in the core of an optical fiber with an embedded scattering medium, from RLs based on fibers with nano- or microstructures, such as in [12,13], which are themselves the scattering medium in the presence of a gain material.

Cellulose-based RLs were first reported in 2002 [14], and since then, several publications have appeared [15–18]. It should be noticed that plasmonically enhanced RLs based on cellulose matrices are reported in Refs. [16,17]. Table 1 summarizes the key features of those publications, including our results, which will be discussed throughout the next sections. The threshold energy for the CNC+Rh6G liquid suspension was determined by experimental analysis and log–log graph for comparison with other literature works.

Among the studied cellulose-based materials, cellulose nanocrystals are especially interesting due to their mechanical

Table 1. Survey of Cellulose-Based Random Lasers[a]

Reference	Scatterer; Gain Medium	Solvent	λ_{exc} (nm); τ_{exc}	λ_{em} (nm)	$\Delta\lambda_{em}$ (nm)	E_{th}
This work	CNC + Rh6G	EG	532; 6 ns	575	10	0.35 mJ 0.075 mJ[b]
This work	HPC + CNC; Rh6G	Flexible thick film	532; 6 ns	575	10	0.30 mJ
[12] de Oliveira *et al*.	AC + PEO; Rh6G	DiCM; meth	532; 6 ns	570	8	97 μJ
[18] Vasileva *et al*.	TW; Rh6G	—	532; 4 ns	—	5-6	0.7 mJ
[17] Zhang *et al*.	HPC + AuNP; Rh6G	Water	532; 30 ps	553	—	4 mJ/cm^2
[16] Dos Santos *et al*.	Flexible (BC) membrane + Si or AgNPs; Rh6G	Solid	532, 6 ns	565	4–10	~ 0.70−2.5 mJ[c]
[15] Viola *et al*.	Paper−Based + TiO_2; RhB	EG, solid	532, 6 ns	587–593	30	~ 0.01−0.1 mJ[d]
[14] Lee and Lawandy	HPC + Kiton Red 620	Water	532, 7 ns	639	5	25 mJ, 41.5°C[e]

[a]HPC, hydroxypropyl cellulose; CNC, cellulose nanocrystaline; AC, acetil cellulose; PEO, polyethylene oxide; EG, ethylene glycol; DiCM, dichloromethane; Meth, methanol; BC, bacterial cellulose; TW, transparent wood; λ_{exc}, excitation wavelength; τ_{exc}, laser excitation pulse width; $\Delta\lambda_{em}$, FWHM; E_{th}, energy threshold.
[b]Value from log-log graph.
[c]Depending on NP concentrations.
[d]Depending on paper circuitry.
[e]Temperature depending threshold.

strength, flexibility, and bio-compatibility, associated with low cost and eco-friendly fabrication processes [3,4].

In this work, we report on alternative RL schemes based on a dye embedded in cellulose nanocrystalline (CNCs) needles as the scattering medium, in suspension, in a liquid or in a flexible 70 μm thick hydroxypropyl cellulose (HPC) film with CNCs.

2. MATERIALS AND METHODS

A. Materials

The CNCs were produced from microcrystalline cellulose from cotton, as reported in Ref. [4]. The resultant aqueous CNC suspension (with 3.2 ± 0.3 wt. % CNC content determined by gravimetric method) was diluted to 0.5 wt. % CNC content and freeze-dried directly (Zirbus, VaCo 2). The resulting white flakes are composed of multiple CNCs, as can be seen in Fig. 1(a).

To obtain the CNC liquid suspension, different amounts of CNCs were added to 2.0 mL of ethylene glycol (EG) (Reagen 99.6%) resulting in a final concentration of CNCs of 1 mg/mL, 3 mg/mL, 5 mg/mL, and 7 mg/mL, respectively, and kept under intense sonication (130 W, Sonics Vibra-Cell CV18) for three 5 min sessions until complete dispersion. Afterwards, 200 μl of a solution of RH6G (10 mM in ethylene glycol) were added to the CNC suspensions. In order to obtain a homogeneous suspension, the final mixtures were put in an ultrasonic bath (Ultracleaner 700) for 5 min.

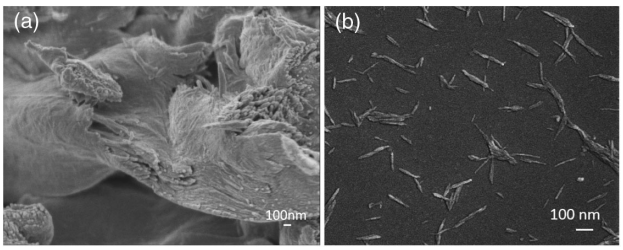

Fig. 1. Images obtained by SEM-FEG (a) of the CNCs as in flakes (macro-sized agglomerates) cross section and (b) of the needles.

To obtain the solid film suspensions, 0.22 g of HPC (Sigma Aldrich 99%, average MW 100.000) and 1.0 mg of CNC were added to 2.0 mL of distilled water and then sonicated (130 W, Sonics Vibra-Cell CV18) for three 5 min sessions for complete dissolution of HPC. Afterwards, 100 μl of a solution of RH6G (4 mM in EG) were added to the HPC ultrasound bath (Ultraclear 700, 50 kHz) for 5 min. The final suspensions were drop casted on polypropylene molds with 3.5 cm × 2.0 cm and dried in an oven at 60°C for ~ 1 h, forming a film with 70 μm thickness. The RL emission measurements were made right after the drying process.

As EG has a higher viscosity when compared to methanol, EG was used here, which allowed the dispersion of a higher concentrations of CNCs in the suspension [19]. Also, there is an influence on the threshold energy by the refractive index of the solvent, as the EG refractive index (1.43) is higher than the methanol refractive index (1.33). A higher energy threshold for the suspension using EG as a solvent is expected [20].

B. SEM Characterization–CNC Needles

In order to confirm the average dimensions of the CNCs, droplets of aqueous suspension of 0.01 wt. % CNCs were deposited onto aluminum stubs and coated with a thin carbon layer (produced with a Q150T ES Quorum sputter coater). The images of CNC flakes were acquired with JEOL JSM 6701F [scanning electron microscope–field emission gun (SEM-FEG)], and the images of individual CNCs with a Carl Zeiss Auriga cross-beam [SEM–focus-ion-beam (FIB)] workstation instruments, operated at 2 kV and 5 kV, respectively. ImageJ software (version 1.45 s) was used to measure these entities, and values of 135 ± 48 nm and 4 ± 1 nm for particles' length and diameter, respectively, were determined for a total 160 measurements for each dimension.

Shown in Fig. 1 are the images obtained with a SEM-FEG and SEM-FIB, presenting the morphology of the CNCs as in

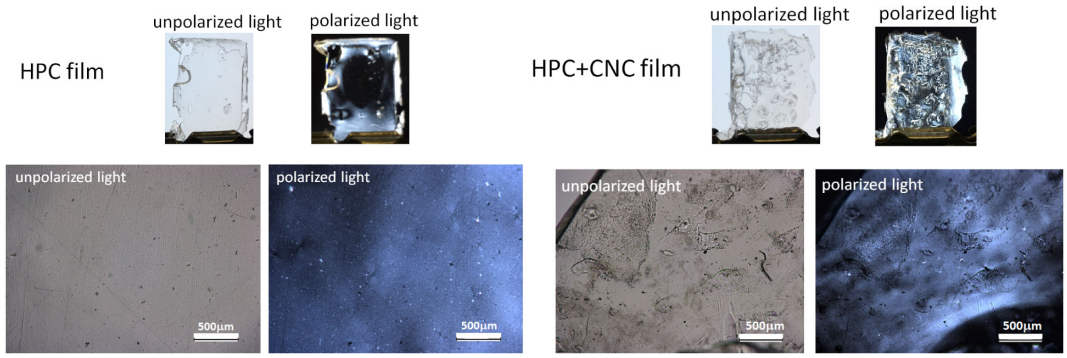

Fig. 2. Digital photographs and light-polarized optical micrographs of HPC and HPC + CNC films.

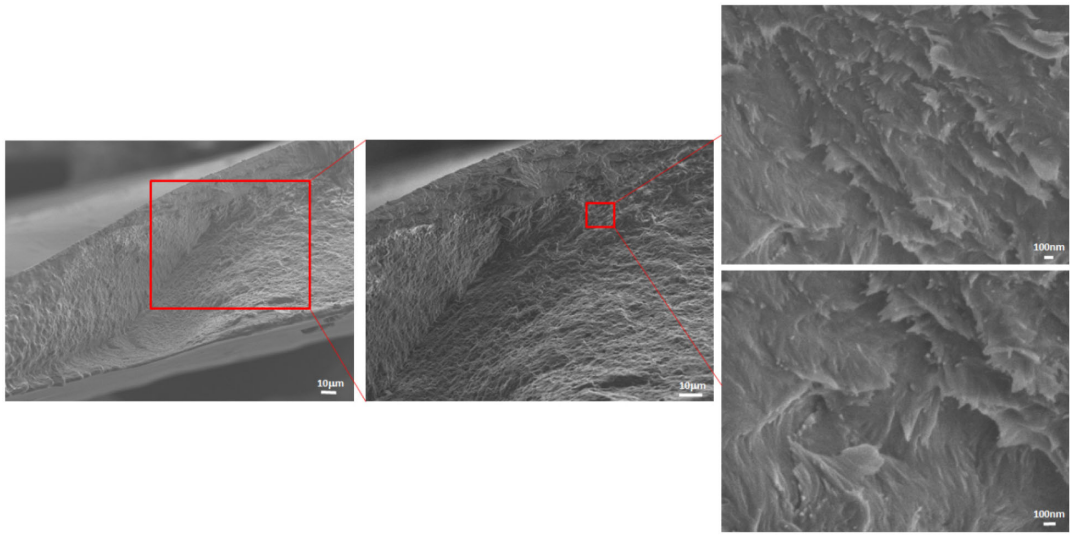

Fig. 3. FEG-SEM micrographs of HPC film containing 5 mg/mL of CNC.

flakes (macro-sized agglomerates) [Fig. 1(a)] and as individual needles [Fig. 1(b)].

The CNC presents flakes formed by nanofibrillated cellulose made according to Ref. [4]. In the CNC flakes, the needles stack up in a self-organized form. In Fig. 1(a), it is also observed that the needles, from a stacking of the fibrillated cellulose, clearly emerge from a cross section of the sample. The needles are the scattering centers of the RL, providing sufficient optical feedback for its operation and high efficiency.

C. HPC + CNC Films

The polarized optical microscopy images (LeicaDM2500 Optical microscope) (Fig. 2) show no evidence of CNC clustering for either system, i.e., HPC or HPC + CNC films, which could influence the results of RL emission. If it were so, polarized light domains will arise from the images, no matter if in the macroscopic or microscopic scale, as observed before in the literature. For instance, in Ref. [4], a hierarchical self-organized cholesteric structure of CNC is observed in pure CNC dried films. In this sense, no such structures were observed for HPC or HPC + CNC films under polarized light, as depicted in the digital photograph and optical micrograph figures (Fig. 2).

The light contrast found in optical microscopy under polarized light for both films is due to the intrinsic birefringence of such composites. Although the films are transparent for visible light, the birefringence emerges as a consequence of the presence of two phases with different refractive indices.

The light-polarized optical microscopy data show that there is no hierarchical clustering of the CNC in the HPC films. However, that does not mean the distribution of the CNC needles is totally random. FEG-SEM images of the HPC + CNC film's cross section (Fig. 3) show the needles mostly are aligned as stacked layers along the longitudinal axis of the film. The images in Fig. 3 were acquired with JEOL JSM 7100FT (SEM-FEG). From the macro scale, such a tendency could be pondered as a long-range morphological organization. Nevertheless, we do not view such organization as a factor, which could have influence on the RL emission properties, once it is not a localized organization.

3. RANDOM LASER CHARACTERIZATION

The lasing emission spectra of the CNCs + Rh6G suspension and the CNC + Rh6G on thick film were measured upon excitation with a pulsed *Q*-switched Nd: YAG laser

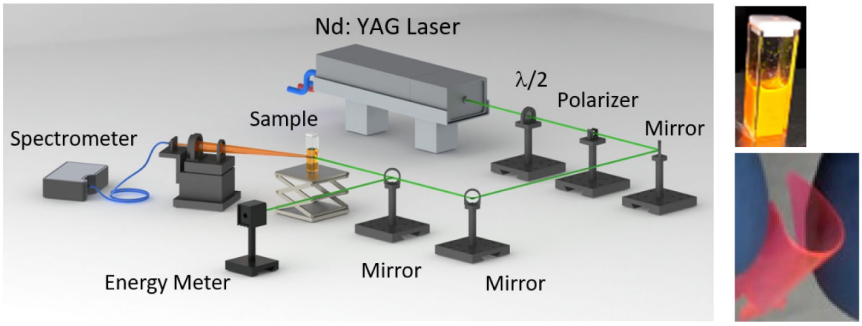

Fig. 4. Experimental setup for the CNC + Rh6G suspension in the cuvette and in the HPC thick-film random laser characterization. The inset shows images of the samples.

(Brio - Quantel, 10 Hertz, 6 ns, $\lambda = 532$ nm). The pump beam carrying a maximum energy of 9 mJ and with a 2.1 mm beam diameter was launched on the sample. A 75 mm convex lens was used to collect the RL emission and direct it onto the spectrometer. The spectral analysis was performed with an Ocean Optics USB4000-UV-VIS spectrometer (spectral resolution ~ 1.5 nm). The measurements of all samples were recorded under identical experimental conditions and carried out at room temperature. Figure 4 shows the experimental setup, the inset shows images of the NCC + Rh6G suspension in the cuvette and in the HPC flexible film.

The excitation light was directed onto the sample in the quartz cuvette at a 45° angle to avoid creating a Fabry–Perot cavity due to reflections on the (10 mm x 10 mm) cuvette walls. Although internal cavities were not easy to excite in the thick film, the same excitation angle geometry was maintained.

4. RESULTS ON RANDOM LASER BEHAVIOR

A. CNCs + Rh6G Suspension

The RL emission from the CNCs + Rh6G suspension is evidenced by a spectral narrowing for samples under different excitation energies (Fig. 5). For all the samples, the linewidth is strongly reduced from 60 nm to 10 nm at its full width at half-maximum (FWHM), from below to well above the threshold for various cellulose concentrations. In the inset in Fig. 5, the narrowing does not occur through the entire spectral emission, but a broad pedestal is still observed for excitation pulse energies above the threshold.

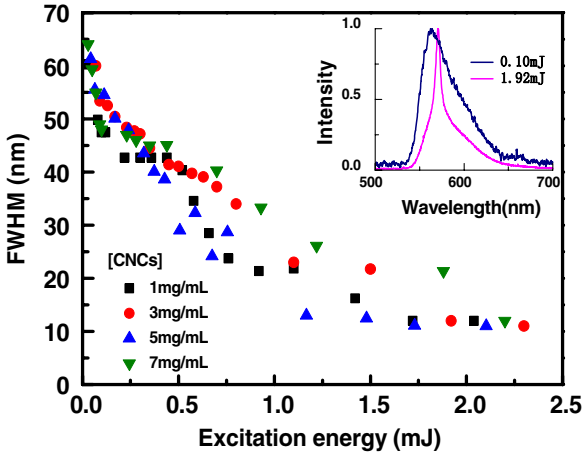

Fig. 5. FWHM of the CNC + Rh6G suspension spectra emission upon laser excitation as a function of excitation energy for samples with different CNC concentrations. The inset shows emission spectra for well below (blue curve) and above (pink curve) threshold energy.

The emitted intensity was affected by the incorporation of more CNCs to the suspension, which in turn affects the scattering in the RL media. Figure 6 shows the emission intensity in a log–log plot in order to reveal the response of the RL for the various CNCs' concentration. As can be seen in the Fig. 6 inset, for 5 mg/mL CNCs, the RL efficiency greatly improves with a threshold of 0.35 mJ, which corresponds to 50% of the energy threshold for the sample with 1 mg/mL CNC. Therefore, the 5 mg/mL is the optimal concentration when compared with the 1 mg/mL, 3 mg/mL, and 7 mg/mL concentrations. Also, increasing the CNC amount above 5 mg/mL increases the threshold value, reducing the laser efficiency.

B. HPC + CNC + Rh6G Flexible Random Laser

The self-supported flexible HPC + CNC + Rh6G RL was characterized and compared with the CNC + Rh6G suspension RL. The results for the linewidth reduction and emitted intensity as a function of input power are shown in Figs. 7(a) and 7(b). It should be noted that the film samples have 10% less CNC needles than in the suspension format, although the energy threshold (0.3 mJ) is similar. Also, the excitation energy for the film sample was increased only up to 1 mJ, due to the degradation of the sample above this energy.

It is important to emphasize that the self-supported film configuration offers more flexibility, and the RL operates with no feedback from any solid substrate. Such a condition, and based on the physical–chemical properties of the start suspension used to cast the films, e.g., viscosity and colloidal stability, allow us to ponder the potential of such a system in manufacturing lab-on-chip fluorescent biosensors. A film as such could replace bulk diodes, usually found in fluorescence-based detection biosensors devices [21].

The concentration of CNCs in the solid suspension was 10.2 mg/cm^3, and in the liquid suspension, the CNC concentrations were 1 mg/cm^3, 3 mg/cm^3, 5 mg/cm^3, and 7 mg/cm^3. Also, the Rh6G concentration in the solid suspension was 4.92×10^{18} molecules/cm^3 and in the liquid

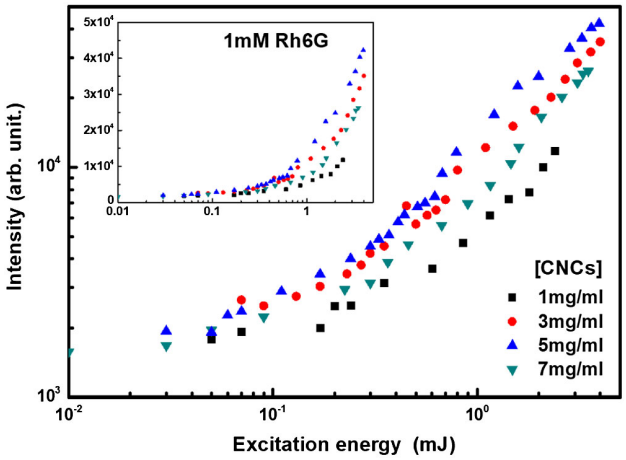

Fig. 6. Random laser emitted intensity as a function of the excitation energy for various CNC concentrations. The inset is a log-linear plot of the emitted intensity as function of the excitation energy for various CNC concentrations.

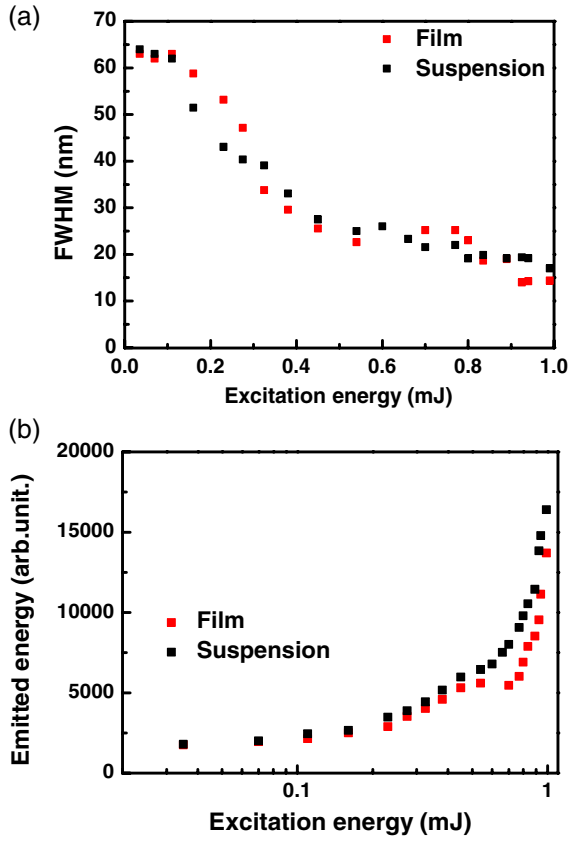

Fig. 7. (a) FWHM and (b) emission intensity as function of the excitation energy for the HPC + CNCs + Rh6G suspension (black square) and thick film (red square). The CNCs' thick-film and suspension concentrations are 0.5 mg and 10 mg, respectively, for the same 4 mM of Rh6G dye concentration.

suspension 5.47×10^{17} molecules/cm^3. Therefore, the concentration of both CNCs and Rh6G is higher in solid than in liquid suspensions. On the other hand, in the thick HPC film, the laser beam interacts in a smaller optical path when compared to the path in the cuvette (1 cm × 1 cm). This reduces the intensity of the Rh6G emission considerably, demonstrating the good scattering properties of the HPC + CNC film, since it has the same threshold value as in the liquid suspension. It was observed that the HPC + Rh6G film had a pink color, which can be associated with a shift at the peak maximum of its absorption band, with respect to the monomer peak position. Such a shift indicates the formation of J-type aggregates. On the liquid suspension, it presents the Rh6G characteristic orange color, and by the absorption spectrum measurement, one can conclude that, besides Rh6G monomers, two types of aggregates occur, i.e., H- and J-type aggregates [22], which leads to a less intense emission. One concludes that for the same threshold energy, the self-supported flexible film needs a shorter optical path and does not favor the formation of both H- and J-type aggregates, thus allowing different applications, as will be discussed in the Conclusion.

5. DISCUSSION

Our results using the novel bio-degradable CNC needles as the scatterers for a dye-based RL can be directly compared to other literature results also using cellulose-based scatterers, as summarized in Table 1. Except for the work of Ref. [17], which employs 30 ps pulses, all the other tabulated works employ 532 nm/4-7 ns long pulses. The lasing bandwidths of all reported RLs are around the same value between 4 nm and 10 nm, except for the work of Ref. [15] (30 nm). In RLs, the bandwidth is determined by the gain medium, which, in the case of dyes, can vary according to the used solvent and excitation wavelength. Therefore, this characteristic is similar among all reported cellulose RLs, including ours. The central emission wavelength follows the same analysis as above. Therefore, except for Kiton Red 620 (emission around 640 nm), all the other rhodamine-based RLs had peak wavelength between 553 nm and 593 nm. Another important parameter is the RL threshold. The threshold value in our work is among the smaller threshold values shown in Table 1. On the other hand, in Ref. [12] where an electrospun polymeric composite was investigated, a threshold energy smaller than all tabulated work is presented; this fact can be attributed to a higher dye + scatterer concentrations and a lower solvent refraction index, which directly affect the threshold energy, as discussed in Ref. [20]. Moreover, for a fluidic paper-based device, this configuration leads to a lower energy threshold [15].

Finally, it should be mentioned that an important and detrimental characteristic of the organic-based RL is the operating lifetime under pumping regime. The degradation of the RL in the thick film configuration was performed by evaluating the variation of the FWHM and the intensity as a function of the number of shots at a known frequency (5 Hz), using the software SpectraSuite 1.6.0_11. The degradation time in our dye-based RL system was similar to other reported in the literature (several 10's of minutes) ([23] and references therein). This can be mitigated or overcome using solid state gain media, such as rare-earth-doped nano/sub-micrometer particles [24] or semiconductor-based nano- or micrometer-sized structures [25].

6. CONCLUSION

In this work, we have investigated two architectures for a RL using various concentrations of CNC needles as scatterers and Rh6G as the gain medium. From the suspension-in-cuvette architecture, an optimized CNC concentration of 5 mg/mL was obtained. We also investigated the RL in a flexible, self-supported 70 μm thick film formed by HPC containing CNCs + Rh6G. The films presented a similar energy threshold when compared to the colloidal suspension, but with 10% less Rh6G than the suspension. Such results point out the potential of such a system in manufacturing lab-on-chip fluorescent biosensors, replacing, for instance, bulk diodes usually found in fluorescence-based detection biosensor devices. Both designs were compared to reported literature work on cellulose-based RLs, with a very good comparison performance.

Funding. Coordenação de Aperfeiçoamento de Pessoal de Nível Superior; Conselho Nacional de Desenvolvimento Científico e Tecnológico; Fundação de Amparo à Ciência e Tecnologia do Estado de Pernambuco; Instituto Nacional de Fotônica (INFo); Office of Naval Research Global; European Regional Development Fund; Fundação para a Ciência e a Tecnologia; Programa Operacional Lisboa 2020; Financiadora de Estudos e Projetos.

Acknowledgment. I.C.S.C. and A.S.L.G. acknowledge support by the Office of Naval Research Global. The authors thank Prof. M. Helena Godinho for the CNC material and for fruitful discussions. It was also funded by FEDER funds through the COMPETE 2020 Program, National Funds through FCT—Portuguese Foundation for Science and Technology and POR Lisboa2020, under the projects with references POCI- 01-0145-FEDER-007688 (Reference UID/CTM/50025), UID/BIA/00329/2013, PTDC/CTM-BIO/6178/2014, M-ERA- NET2/0007/2016 (CellColor), and PTDC/CTM-REF/30529/2017(NanoCell2SEC). I.C.S. Carvalho acknowledges Mr. Fredy G.O. Gutiérrez for technical support. The authors are grateful to CBPF for the use of the facilities for electron microscopy in the LabNano/CBPF, Rio de Janeiro-BR (JEOL JSM-7100FT), and the laboratory VDG-PUC-Rio for the use of the facilities for electron microscope SEM-FEG JEOL JSM6701F.

Disclosures. The authors declare no conflicts of interest.

[†]These authors contributed equally to this work.

REFERENCES

1. R. J. Moon, A. Martini, J. Nairn, J. Simonsen, and J. Youngblood, "Cellulose nanomaterials review: structure, properties and nanocomposites," Chem. Soc. Rev. **40**, 3941–3994 (2011).
2. S. Caixeiro, M. Peruzzo, O. D. Onelli, S. Vignolini, and R. Sapienza, "Disordered cellulose-based nanostructures for enhanced light scattering," ACS Appl. Mater. Interfaces **9**, 7885–7890 (2017).
3. D. Gaspar, S. N. Fernandes, A. G. De Oliveira, J. G. Fernandes, P. Grey, R. V. Pontes, L. Pereira, R. Martins, M. H. Godinho, and E. Fortunato, "Nanocrystalline cellulose applied simultaneously as the gate dielectric and the substrate in flexible field effect transistors," Nanotechnology **25**, 094008 (2014).
4. S. N. Fernandes, P. L. Almeida, N. Monge, L. E. Aguirre, D. Reis, C. L. P. de Oliveira, A. M. F. Neto, P. Pieranski, and M. H. Godinho, "Mind the microgap in iridescent cellulose nanocrystal films," Adv. Mater. **29**, 1603560 (2017).
5. F. Luan, B. Gu, A. S. L. Gomes, K. T. Yong, S. Wen, and P. N. Prasad, "Lasing in nanocomposite random media," Nano Today **10**(2), 168–192 (2015).
6. L. Sznitko, J. Mysliwiec, and A. Miniewicz, "The role of polymers in random lasing," J. Polym. Sci. B **53**, 951–974 (2015).
7. S. F. Yu, "Electrically pumped random lasers," J. Phys. D **48**, 483001 (2015).
8. N. M. Lawandy, R. M. Balachandran, A. S. L. Gomes, and E. Sauvain, "Laser action in strongly scattering media," Nature **368**, 436–438 (1994).
9. V. S. Lethokhov, "Generation of light by a scattering a medium with a negative resonance absorption," Sov. Phys. JETP **40**, 835–840 (1968).
10. C. J. S. De Matos, L. de Souza Menezes, A. M. Brito-Silva, M. A. M. Gámez, A. S. L. Gomes, and C. B. De Araújo, "Random fiber laser," Phys. Rev. Lett. **99**, 153903 (2007).
11. D. V. Churkin, S. Sugavanam, I. D. Vatnik, Z. Wang, E. V. Podivilov, S. A. Babin, Y. Rao, and S. K. Turitsyn, "Recent advances in fundamentals and applications of random fiber lasers," Adv. Opt. Photon. **7**, 516–569 (2015).
12. M. C. A. de Oliveira, L. de Souza Menezes, P. I. R. Pincheira, C. Rojas-Ulloa, N. R. Gomez, H. P. de Oliveira, and A. S. Leônidas Gomes, "A random laser based on electrospun polymeric composite nanofibers with dual-size distribution," Nanoscale Adv. **1**, 728–734 (2019).
13. G. Lv, D. Huang, S. Wu, G. Ren, W. Yang, and T. Li, "Random lasing action generation in polymer nanofiber with small diameters," Laser Phys. **28**, 075803 (2018).
14. K. Lee and N. M. Lawandy, "Laser action in temperature-controlled scattering media," Opt. Commun. **203**, 169–174 (2002).
15. I. Viola, N. Ghofraniha, A. Zacheo, V. Arima, C. Conti, and G. Gigli, "Random laser emission from a paper-based device," J. Mater. Chem. C **1**, 8128–8133 (2013).
16. M. V. Dos Santos, C. T. Dominguez, J. V. Schiavon, H. S. Barud, L. S. A. De Melo, S. J. L. Ribeiro, A. S. L. Gomes, and C. B. De Araújo, "Random laser action from flexible biocellulose-based device," J. Appl. Phys. **115**, 083108 (2014).
17. R. Zhang, S. Knitter, S. F. Liew, F. G. Omenetto, B. M. Reinhard, H. Cao, and L. Dal Negro, "Plasmon-enhanced random lasing in bio-compatible networks of cellulose nanofibers," Appl. Phys. Lett. **108**, 011103 (2016).
18. E. Vasileva, Y. Li, I. Sychugov, M. Mensi, L. Berglund, and S. Popov, "Lasing from organic dye molecules embedded in transparent wood," Adv. Opt. Mater. **5**, 1700057 (2017).
19. L. Yang, G. Feng, J. Yi, K. Yao, G. Deng, and S. Zhou, "Effective random laser action in rhodamine 6G solution with Al nanoparticles," Appl. Opt. **50**, 1816–1821 (2011).
20. J. Yi, G. Feng, L. Yang, K. Yao, C. Yang, Y. Song, and S. Zhou, "Behaviors of the Rh6G random laser comprising solvents and scatterers with different refractive indices," Opt. Commun. **285**, 5276–5282 (2012).
21. N. M. M. Pires, T. Dong, U. Hanke, and N. Hoivik, "Recent developments in optical detection technologies in lab-on-a-chip devices for biosensing applications," Sensors **14**, 15458–15479 (2014).
22. M. Lofaj, I. Valent, and J. Bujdák, "Mechanism of rhodamine 6G molecular aggregation in montmorillonite colloid," Central Eur. J. Chem. **11**, 1606–1619 (2013).
23. P. I. R. Pincheira, A. F. Silva, S. I. Fewo, S. J. M. Carreño, A. L. Moura, E. P. Raposo, A. S. L. Gomes, and C. B. de Araújo, "Observation of photonic paramagnetic to spin-glass transition in a specially designed TiO_2 particle-based dye-colloidal random laser," Opt. Lett. **41**, 3459–3462 (2016).
24. A. L. Moura, L. J. Q. Maia, A. S. L. Gomes, and C. B. de Araújo, "Optimal performance of $NdAl_3(BO_3)_4$ nanocrystals random lasers," Opt. Mater. **62**, 593–596 (2016).
25. M. L. da Silva-Neto, M. C. A. T. Dominguez, R. E. M. Lins, N. Rakov, C. B. de Araújo, L. de Souza Menezes, H. P. de Oliveira, and A. S. L. Gomes, "UV random laser emission from flexible ZnO-Ag-enriched electrospun cellulose acetate fiber matrix," Sci. Rep. **9**, 11765 (2019).